Available online at www.sciencedirect.com

ScienceDirect

Geochimica et Cosmochimica Acta 164 (2015) 284–297

Geochimica et Cosmochimica Acta

www.elsevier.com/locate/gca

Theoretical calculation of nitrogen isotope equilibrium exchange fractionation factors for various NO_y molecules

Wendell W. Walters [a,*], Greg Michalski [a,b]

[a] Department of Earth, Atmospheric, and Planetary Sciences, Purdue University, 550 Stadium Mall Drive, West Lafayette, IN 47907, United States

[b] Department of Chemistry, Purdue University, 560 Oval Drive, West Lafayette, IN 47907, United States

Received 30 March 2015; accepted in revised form 14 May 2015; available online 22 May 2015

Abstract

The nitrogen stable isotope ratio ($^{15}N/^{14}N$) of nitrogen oxides ($NO_x = NO + NO_2$) and its oxidation products ($NO_y = NO_x + PAN$ (peroxyacetyl nitrate $= C_2H_3NO_5$) $+ HNO_3 + NO_3 + HONO + N_2O_5 + \cdots +$ particulate nitrates) has been suggested as a tool for partitioning NO_x sources; however, the impact of nitrogen (N) equilibrium isotopic fractionation on $^{15}N/^{14}N$ ratios during the conversion of NO_x to NO_y must also be considered, but few fractionation factors for these processes have been determined. To address this limitation, computational quantum chemistry calculations of harmonic frequencies, reduced partition function ratios ($^{15}\beta$), and N equilibrium isotope exchange fractionation factors ($\alpha_{A/B}$) were performed for various gaseous and aqueous NO_y molecules in the rigid rotor and harmonic oscillator approximations using the B3LYP and EDF2 density functional methods for the mono-substitution of ^{15}N. The calculated harmonic frequencies, $^{15}\beta$, and $\alpha_{A/B}$ are in good agreement with available experimental measurements, suggesting the potential to use computational methods to calculate $\alpha_{A/B}$ values for N isotope exchange processes that are difficult to measure experimentally. Additionally, the effects of solvation (water) on $^{15}\beta$ and $\alpha_{A/B}$ were evaluated using the IEF-PCM model, and resulted in lower $^{15}\beta$ and $\alpha_{A/B}$ values likely due to the stabilization of the NO_y molecules from dispersion interactions with water. Overall, our calculated $^{15}\beta$ and $\alpha_{A/B}$ values are accurate in the rigid rotor and harmonic oscillator approximations and will allow for the estimation of $\alpha_{A/B}$ involving various NO_y molecules. These calculated $\alpha_{A/B}$ values may help to explain the trends observed in the N stable isotope ratio of NO_y molecules in the atmosphere.

1. INTRODUCTION

The family of oxidized nitrogen molecules in the atmosphere, denoted as NO_y, which includes the sum of nitrogen oxides ($NO_x = NO + NO_2$) and its oxidation products ($NO_y = NO_x + PAN$ (peroxyacetyl nitrate $= C_2H_3NO_5$) $+ HNO_3 + NO_3 + HONO + N_2O_5 + \ldots +$ particulate nitrates) (Logan, 1983), are environmentally-relevant molecules that play a crucial role in many atmospheric processes (Solomon et al., 2007). In the troposphere, NO_x controls the concentrations of ozone (O_3) and the hydroxyl radical (OH), and is primarily oxidized to form nitrate aerosols ($NO_3^-{}_{(s)}$) and nitric acid (HNO_3) (Crutzen, 1979; Lawrence and Crutzen, 1999; Atkinson, 2000). Subsequent wet and/or dry deposition of HNO_3 leads to numerous deleterious environmental impacts, including degradation of drinking water, soil acidification, eutrophication, and biodiversity changes in terrestrial ecosystems (Galloway et al., 2004). During the nighttime, the nitrate radical (NO_3) is a major atmospheric oxidant, influencing the lifetime of various other trace gases (Wayne et al.,

* Corresponding author. Tel.: +1 (765) 496 4906; fax: +1 (765) 496 1210.

E-mail address: waltersw@purdue.edu (W.W. Walters).

http://dx.doi.org/10.1016/j.gca.2015.05.029

0016-7037/

1991). Reactions involving volatile organic compounds (VOCs) and NO_2 can lead to the formation of PAN, which can be transported over relatively large distances and introduce NO_x to pristine environments (Nielsen et al., 1981). In the stratosphere, HNO_3 is the primary component of polar stratospheric clouds (PSCs) that form by the reactions of dinitrogen pentoxide (N_2O_5) and chlorine nitrate ($ClONO_2$) on the surface of stratospheric cloud particles in Polar Regions (Crutzen and Arnold, 1986; Voigt et al., 2000). PSCs provide a surface for heterogeneous chemical reactions to occur which leads to ozone destruction in the stratosphere (Solomon, 1999).

In general, the precursor to the formation of NO_y is the emission of NO_x that is subsequently oxidized by various atmospheric oxidants such as O_3, OH, NO_3, HO_2, and the organoperoxy radicals (RO_2). Due to the important impacts NO_y molecules have on the environment, it is important to understand the sources of NO_x and the processes that transform it into NO_y. While significant efforts have been made to reduce the NO_x emission from stationary and mobile sources (Melillo and Cowling, 2002), there are still relatively large uncertainties in the total NO_x emission budget, both natural and anthropogenic, estimated between 30% and 50% (Galloway et al., 2004). In order to better estimate the relative importance of various NO_x sources to the overall NO_x emission budget, the analysis of the nitrogen (N) stable isotope ratio ($^{15}N/^{14}N$) of atmospherically derived HNO_3 and NO_3^- from wet and/or dry deposition has been suggested as a possible tool for partitioning NO_x sources (Elliott et al., 2007), because various NO_x sources have relatively distinct $^{15}N/^{14}N$ ratios (Moore, 1977; Heaton, 1990; Ammann et al., 1999; Pearson et al., 2000; Li and Wang, 2008; Felix et al., 2012; Redling et al., 2013; Felix and Elliott, 2014; Fibiger et al., 2014; Walters et al., 2015). Therefore, if the $^{15}N/^{14}N$ ratios of NO_x are preserved when oxidized to NO_3^- and HNO_3, they can be used as a proxy for NO_x source partitioning. However, implementation of this method requires knowledge of how kinetic and equilibrium isotopic fractionations impacts $^{15}N/^{14}N$ ratios during the conversion of NO_x to NO_y (Freyer, 1978; Freyer et al., 1993). If these factors are considerable, then they may limit the utility of using $^{15}N/^{14}N$ ratios of NO_x for source partitioning. Yet, few fractionation factors for this conversion have been determined.

The transformation of NO_x to HNO_3 is a complicated process that involves several different reaction pathways (Scheme 1) (Seinfeld and Pandis, 2006). During this transformation, various NO_y molecules exist in equilibrium and are likely to undergo isotope exchange reactions involving the N isotopologues such as the exchange of NO and NO_2 (Eq. (1)):

$$^{15}NO + {}^{14}NO_2 \leftrightarrow {}^{14}NO + {}^{15}NO_2 \quad (1)$$

A field study has indicated that this equilibrium isotope exchange may have a strong influence on the observed $^{15}N/^{14}N$ ratios in atmospheric NO and NO_2 (Freyer et al., 1993), suggesting that isotope exchange equilibrium may play a significant role in influencing the $^{15}N/^{14}N$ ratios of various NO_y molecules. In order to fully understand

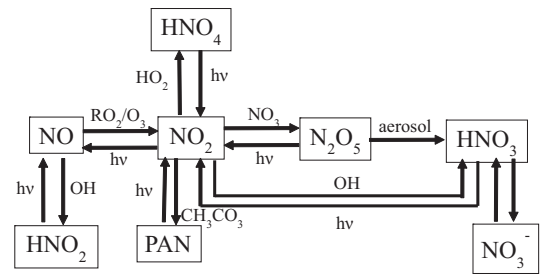

Scheme 1. Various transformation pathways for NO_x to HNO_3.

studies of the N isotopic composition of atmospherically derived NO_y compounds (Freyer, 1978; Elliott et al., 2007, 2009; Hastings et al., 2009; Mara et al., 2009; Geng et al., 2014; Beyn et al., 2015), the effects of isotope exchange on $^{15}N/^{14}N$ ratios involving NO_y molecules needs to be addressed.

Previous studies have calculated equilibrium isotope exchange fractionation factors involving several NO_y molecules based on experimental measurements of harmonic frequencies (Begun and Fletcher, 1960; Richet et al., 1977) and on empirical force field methods (Monse et al., 1969). However, equilibrium isotope exchange fractionation factors have not been determined for all atmospherically relevant NO_y molecules including but not limited to: NO_3, N_2O_5, halogen nitrates ($XONO_2$), and PAN due primarily to the absence of spectroscopic data for ^{15}N isotopologues of these NO_y molecules. Recently, computational quantum chemistry methods have been used to calculate equilibrium isotope exchange fractionation factors for H and O (Driesner et al., 2000), Li (Yamaji et al., 2001), B (Oi, 2000; Oi and Yanase, 2001), Cr (Schauble et al., 2004), Fe (Anbar et al., 2005), Cu (Seo et al., 2007), Mo (Tossell, 2005), and S (Otake et al., 2008). Here we use computational quantum chemistry methods to calculate equilibrium isotope exchange fractionation factors for the major NO_y molecules that are suspected to exist in equilibrium and compare them to experimental and prior theoretical determinations.

2. METHODS AND THEORY

2.1. Calculation of equilibrium isotope exchange fractionation factors

Early treatment of equilibrium isotope exchange factors were reported in 1947 by Urey in terms of isotopic partition function ratios, and by Bigeleisen and Mayer who introduced the isotopic reduced partition function ratio (RPFR) now in general use (Bigeleisen and Mayer, 1947; Urey, 1947). Assuming the Born–Oppenheimer and harmonic oscillator approximations, the RPFR (denoted as β) is written as (Eq. (2)):

$$\beta = \left(\frac{s_2}{s_1}\right)_f = \prod_i^N \frac{\mu_{2i}}{\mu_{1i}} \times \exp\left(\sum_i^N \frac{\mu_{1i}-\mu_{2i}}{2}\right) \times \prod_i^N \frac{1-\exp(-\mu_{1i})}{1-\exp(-\mu_{2i})} = (CF)(ZPE)(EXC) \quad (2)$$

In Eq. (2), subscripts 1 and 2 refer to the light and heavy isotopologue respectively, $\mu_i = hc\nu_i/kT$, h is Planck's

constant, c is speed of light, v_i is vibrational frequency, k is Boltzmann constant, T is temperature, N refers to the normal mode frequencies (3N-6 or 3N-5 if linear), and s_1 and s_2 are symmetry numbers that do not lead to any isotope effect but must be considered from a statistical perspective. Eq. (2) points out that β can be considered the product of a classical factor (CF) that accounts for translational and rotational energy, the zero point energy contribution (ZPE), and an excitation factor (EXC). For an equilibrium isotope exchange reaction (Eq. (3)):

$$A_1 + B_2 \leftrightarrow A_2 + B_1 \tag{3}$$

where A and B are different chemical species, and subscripts 1 and 2 again refer to the light and heavy isotopologue respectively, the reduced equilibrium constant, written as $K_{A/B}$, and also defined as the equilibrium isotope fractionation factor ($\alpha_{A/B}$), can be obtained from the β of A and B (Eq. (4)):

$$K_{A/B} = \alpha_{A/B} = \beta_A/\beta_B \tag{4}$$

By this notation, the equilibrium constant for $NO_2 \leftrightarrow NO$ isotope exchange between ^{14}N and ^{15}N isotopologue pairs (Eq. (1)) is written as (Eq. (5)):

$$K_{NO_2/NO} = {}^{15}\alpha_{NO_2/NO} = \left(\frac{^{15}N}{^{14}N}\right)NO_2 \Big/ \left(\frac{^{15}N}{^{14}N}\right)NO = {}^{15}\beta_{NO_2}/{}^{15}\beta_{NO} \tag{5}$$

Neglecting the symmetry-number factor, since the purely classical symmetry numbers cannot lead to isotope fractionation (Michalski and Bhattacharya, 2009), $\alpha_{A/B}$ only depends on the isotopic dependent vibrational frequencies. Therefore, if the N isotopologue vibrational frequencies are known for various NO_y molecules, theoretical equilibrium isotope exchanges involving NO_y molecules can be calculated in the rigid rotor and harmonic oscillator approximations. Theoretically, for proper use of the Bigeleisen–Mayer equation (Eq. (2)) for β calculations, pure harmonic vibrational frequencies must be used to satisfy the approximations used within the Teller–Redlich product rule (Liu et al., 2010). Isotopologue harmonic frequencies have been obtained from experimental spectroscopic data for many di- and some tri- atomic molecules, but few have been experimentally determined for larger molecules or radicals because of challenges in isotopologue synthesis. However, they can be calculated using computational quantum chemistry methods.

2.2. Computational chemistry methods

The optimized geometries (bond angles and bond lengths) and harmonic frequencies were calculated for the following nineteen NO_y molecules: NO, NO_2, NO_3, NO_3^-, HNO_3, PAN, N_2O_5, $ClONO_2$, nitrite anion (NO_2^-), nitrous acid (HONO), peroxynitric acid (HNO_4), dinitrogen trioxide (N_2O_3) dinitrogen tetroxide (N_2O_4), nitrous oxide (N_2O), nitryl bromide ($BrNO_2$), nitryl chloride ($ClNO_2$), bromine nitrate ($BrONO_2$), nitrosyl chloride (NOCl), and nitrosyl bromide (NOBr) using computational quantum chemistry methods. The masses that correspond to the most abundant naturally occurring isotopes of elements (^1H, ^{12}C, ^{14}N, ^{16}O, ^{35}Cl, and ^{79}Br) and the mono-substitution of ^{15}N for ^{14}N were used in the harmonic frequency calculations. All calculations were performed with the Q-Chem 4.2 program suite (Shao et al., 2015) using both the B3LYP (Lee et al., 1988; Becke, 1993) and EDF2 (Lin et al., 2004) hybrid density functional theory (DFT) methods, with the latter method specifically optimized for harmonic frequency calculations. DFT calculations are not strictly first-principle methods, but include some of the electron correlation accounting for the instantaneous interactions of pairs of electrons at a favorable computational cost (Jensen, 1999). For each method, the Dunning correlation-consistent polarized valence triple ζ (cc-pVTZ) basis set was used (Dunning, 1989).

Computational methods for calculating harmonic frequencies are obtained from the force constant matrix (second derivative of the energy) evaluated at the equilibrium geometry (Jensen, 1999), and are generally larger than the experimentally observed harmonic frequencies, due to incomplete incorporation of electron correlation and the use of finite basis sets (Foresman and Frisch, 1996). To check the accuracy of our chosen levels of theory, harmonic frequencies were calculated for both B3LYP/cc-pVTZ and EDF2/cc-pVTZ and compared with experimental harmonic frequencies for a variety of di- and tri- atomic molecules that included: NO, NO_2, N_2, N_2O, carbon dioxide (CO_2), water (H_2O), carbonyl sulfide (OCS), sulfur dioxide (SO_2), disodium (Na_2), hydrogen cyanide (HCN), nitrogen monohydride (NH), dilithium (Li_2), hydroxyl radical (OH), carbon disulfide (CS_2), and hydrogen sulfide (H_2S) for a total of 37 vibrational modes covering a harmonic frequency range of 159.08–3938.74 cm^{-1}. A least squares linear regression fitting was applied to relate calculated harmonic frequencies to experimental values for each DFT method in order to assess their accuracy and to determine a scale factor which was subsequently used to scale all calculated vibrational frequencies to more closely match experimental values.

2.3. Determination of NO_y $^{15}\beta$ and $\alpha_{A/B}$ values

The scaled harmonic frequencies for both DFT methods were used to calculate $^{15}\beta$ values for each NO_y isotopologue. In the case of N_2O and N_2O_3, positionally dependent ^{15}N substitution was taken into account in the calculations of $^{15}\beta$, and the geometric average $^{15}\beta$ value was determined. For all other NO_y molecules in which there are multiple N atoms, the N atoms were ruled equivalent due to molecular symmetry. To the best of our knowledge, $^{15}\beta$ values have not previously been calculated for NO_3, HNO_4, N_2O_5, PAN, $ClONO_2$, and $BrONO_2$. To assess the accuracy of our calculated $^{15}\beta$ values, they were compared to $^{15}\beta$ values calculated from experimental harmonic frequencies and/or calculated using empirical force field methods for NO (Monse et al., 1969; Richet et al., 1977), NO_2 (Monse et al., 1969; Richet et al., 1977), N_2O (Bigeleisen and Friedman, 1950; Chedin et al., 1976), and HNO_3 (Monse et al., 1969). Using our calculated $^{15}\beta$ values, $\alpha_{A/B}$ were calculated for the following gaseous exchange processes ($A \leftrightarrow B$): $NOCl \leftrightarrow NO$, $HNO_2 \leftrightarrow NO$, $N_2O_5 \leftrightarrow NO_2$,

$N_2O_4 \leftrightarrow NO_2$, $ClONO_2 \leftrightarrow NO_2$, $PAN \leftrightarrow NO_2$, and $HNO_3 \leftrightarrow NO$ in the temperature range from 150 to 450 K. The thermodynamic energy that governs the equilibrium isotope exchange for a particular isotopologue arises due to small differences in the vibrational energies of isotopically substituted molecules (Urey, 1947). NO_y molecules that have been substituted with a heavier N isotope (^{15}N) will vibrate at lower frequencies than NO_y molecules containing the more common light N isotope (^{14}N). The relative lower vibrational frequency for ^{15}N containing molecules will reduce the vibrational zero-point energy (ZPE,=1/2Σhν for harmonic oscillators) compared to ^{14}N containing molecules. The reduction of vibrational ZPE for a ^{15}N containing molecule will be greater for a particular N-bearing molecule that depends on the strength of bonds that N is involved in, and this will drive the direction of an N isotope equilibrium exchange. For example, in the N isotopologue equilibrium exchange between NO and NO_2 (Eq. (1)), the vibrational ZPEs are 11.35, 11.15, 22.41, and 21.04 kJ/mol for ^{14}NO, ^{15}NO, $^{14}NO_2$, and $^{15}NO_2$ respectively (Begun and Fletcher, 1960). Because the difference in the vibrational ZPE is greater for NO_2 with the substitution of ^{15}N ($\Delta ZPE = 0.37$ kJ/mol) than it is for NO ($\Delta ZPE = 0.20$ kJ/mol), this will drive the equilibrium isotope exchange between NO and NO_2 (Eq. (1)) to the right, because the total vibrational ZPE for the right-hand side is lower by approximately 0.16 kJ/mol than the vibrational ZPE on the left-hand side. Consequently, at equilibrium between NO and NO_2, there will be a greater abundance of ^{14}NO and $^{15}NO_2$ than would be expected if N isotopes were randomly distributed. Several of our calculated $\alpha_{A/B}$ were compared to those calculated in previous studies using empirical force field methods (Monse et al., 1969), experimental harmonic frequencies (Richet et al., 1977) and/or experimentally measured. (Leifer, 1940; Begun and Melton, 1956; Yeatts, 1958; Brown and Begun, 1959; Kauder et al., 1959). Here we consider a handful of NO_y exchange process, but many other $\alpha_{A/B}$ may be determined using our calculated $^{15}\beta$ values.

2.4. Solvent effects

A solvent can have a major impact on equilibrium constants, reaction rates, and molecular properties (Lasaga, 1990, 1998), and several NO_y compounds are important in gas-aqueous exchange chemistry. Computational quantum chemistry methods treat solvent effects by inclusion of a continuum solvent model, referred as Self-Consistent Reaction Field (SCRF) (Jensen, 1999). In these type of models, a potential energy term, V_{solv}, is added to the molecular electronic Hamiltonian, and the solvent is treated as a continuous dielectric surrounding a cavity that contains the solute molecule ignoring the detailed molecular structure of the solvent (Tomasi and Persico, 1994). To obtain $V_{solv,}$ charges are placed on various parts of the cavity surface and the effect of the electrostatic field on both the polarization of the dielectric continuum, and the electric moments of the molecule are calculated, with the charges themselves depending on the solute electrons and nuclei in a self-consistent manner. The key quantities that define this solvent continuum are the dielectric constant, ε (Robinson and Stokes, 1959), and cavity shape (Tomasi and Persico, 1994).

Various methods exists for the quantum mechanical calculation of solvent effects that depend on the models description of the cavity (Jensen, 1999). In the widely used Polarizable Continuum Solvation Model (PCM), a sphere shaped cavity of radius 1.2 times the Van der Waal's radius around each atom of the molecule is used (Tomasi and Persico, 1994). Charges are placed on the surface of the cavity resulting from intersecting spheres to simulate the external field of the solvent (Tomasi and Persico, 1994). PCM improves upon early solvent models by providing a more realistic description of molecular shape and using the exact electron density of the solute to polarize the continuum. Various PCM models exists such as the conductor-like models known as COSMO (Klamt and Schüürmann, 1993), GCOSMO (Truong and Stefanovich, 1995) or C-PCM (Barone and Cossi, 1998; Cossi et al., 2003) as well as more sophisticated models such as the surface and simulation of volume polarization for electrostatics known as the SS(V)PE approach (Chipman, 2000) or equivalently known as the integral equation formalism (IEF-PCM) (Cancès et al., 1997), which provides an exact treatment of the surface polarization. Previous studies have successfully applied PCM models to predict fractionation factors for boron (Liu and Tossell, 2005), iron (Anbar et al., 2005), and sulfur (Otake et al., 2008).

In this study we used the IEF-PCM to investigate the solvent effect on $^{15}\beta$ of eight soluble NO_y molecules that included: HNO_2, HNO_3, HNO_4, N_2O_3, N_2O_4, N_2O_5, NO_2^-, and NO_3^-. The IEF-PCM model was incorporated in the geometry optimization and harmonic frequency calculations of these molecules using both B3LYP/cc-pVTZ and EDF2/cc-pVTZ levels of theory, and $^{15}\beta$ values were calculated in the temperature range of 150–450 K. The key parameter that determines the solvent effect for the IEF-PCM is the dielectric constant, ε, and for our calculations was set to 78.39 which is the value for water at 298 K (Malmberg and Maryott, 1956). While ε of water might vary slightly over the temperature ranged considered in our $^{15}\beta$ calculations, previous studies have shown that this slight variation has minimal to no impact on the calculated β (Otake et al., 2008). To assess the solvent effect, $\alpha_{A/B}$ between gaseous and aqueous phases was calculated for these eight NO_y molecules, and equilibrium N isotope exchange processes involving aqueous phase molecules were compared with experimentally determined values as well as those calculated from previous theoretical studies.

3. RESULTS AND DISCUSSION

3.1. Experimental vs calculated harmonic frequencies

Fig. 1 compares the calculated harmonic frequencies obtained from the B3LYP/cc-pVTZ and the EDF2/cc-pVTZ levels of theory with those experimentally determined for a variety of molecules (Chedin et al., 1976; Richet et al., 1977; Irikura, 2007). The calculated harmonic frequencies and the experimentally harmonic frequencies

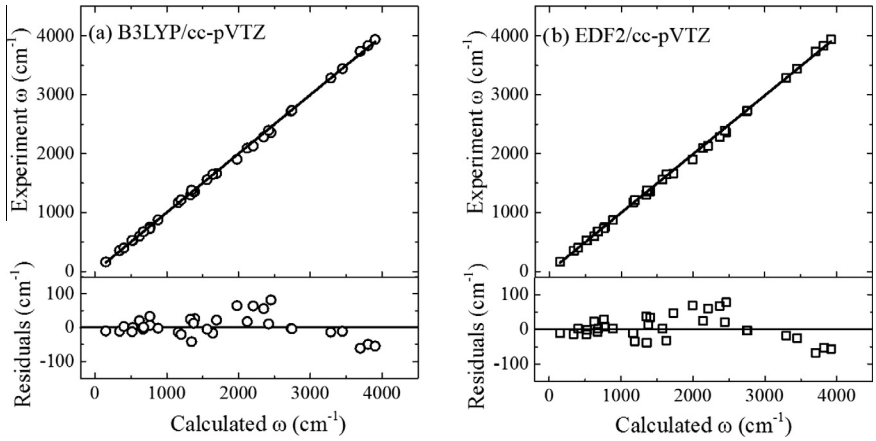

Fig. 1. The least-squares fitting of experimental harmonic frequencies (ω) vs. calculated harmonic frequencies and residuals for (a) B3LYP/cc-pVTZ and (b) EDF2/cc-pVTZ levels of theory.

for these molecules are presented in the Supplementary material (Table S1). The linear fittings of experimental vs. calculated harmonic frequencies (Fig. 1), have slopes of 0.995(±0.003) and 0.990(±0.003) and R^2 values of 0.9997 and 0.9996 for B3LYP/cc-pVTZ and EDF2/cc-pVTZ levels of theory respectively. The slope for each respective level of theory was used to scale all calculated harmonic frequencies with the aim of predicting more accurate values. In general, the scaled harmonic frequencies are in good agreement with observations; however, small differences between the scaled and the experimental harmonic frequencies still exist (Fig. 1). These discrepancies are caused by either the inadequacy of the level of theory used or by experimental error (Liu et al., 2010). Measurement of a molecule's IR or Raman vibrational spectra can be difficult without using a condensed vapor or trapping the molecules in inert matrices, which may lead to interferences. These types of interferences do not apply to computational methods in which harmonic frequencies are calculated for a single molecule in vacuum. Only the most abundant isotopes for elements were used when calculating the harmonic frequency scale factors, but it is important to note that if the harmonic frequencies calculated for the most abundant isotopologue are accurate, then those for other isotopologues are guaranteed to be accurate as well, because any shift in frequencies due to mass occurs only from changes in the mass term in front of the potential matrix term (Otake et al., 2008) (Eq. (6)):

$$\frac{1}{\sqrt{m_i m_j}} \frac{\delta^2 V}{\delta x_i \delta y_i} \tag{6}$$

where V is the potential energy, and m_i ad m_j are the masses of the atoms with coordinate x_i and y_j, respectively. In Eq. (6), it is clear that the accuracy of the computed harmonic frequencies depend only on the $\delta^2 V/\delta x_i \delta y_i$ term, and the change in mass will not directly impact this term. Overall, we feel that the scaled harmonic frequencies are quite accurate and should allow for the determination of the harmonic frequencies for the various N isotopologue NO_y molecules of interest in this study.

3.2. Calculated NO_y harmonic frequencies

The scaled harmonic frequencies calculated using B3LYP/cc-pVTZ and EDF2/cc-pVTZ levels of theory for gaseous N isotopologue molecules are presented in a table in the Supplementary material (Table S2). In general, there is excellent agreement between the two DFT methods used to calculate harmonic frequencies; they are within 0.3 and 21.5 cm^{-1} for each vibrational mode (Fig. 2), indicating that both DFT methods calculated similar potential matrix terms (Eq. (6)). The only exception to this general agreement was for NO_3 in which the two DFT methods computed harmonic frequencies that differed by up to 136.6 cm^{-1} (Fig. 2), signifying a disagreement in the calculated potential matrix terms (Eq. (6)). Previous computational quantum chemistry studies on NO_3 have indicated the difficulty in calculating accurate geometries and

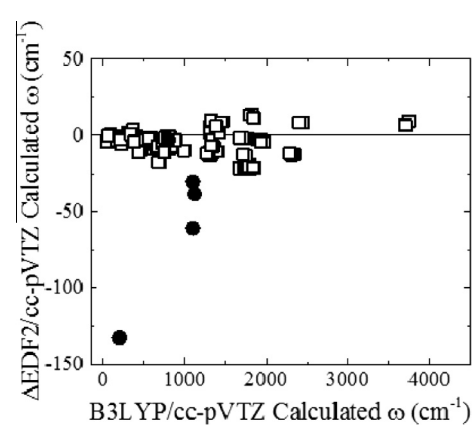

Fig. 2. Comparison of calculated B3LYP/cc-pVTZ harmonic frequencies (ω) with the difference between B3LYP/cc-pVTZ and EDF2/cc-pVTZ calculated harmonic frequencies (ΔEDF2). The circle points represent the frequencies calculated for NO_3, and the square points represent all other frequencies calculated for every NO_y molecule included in this study.

therefore vibrational frequencies due to it being a polyatomic doublet radical (Morris et al., 1990; Dutta et al., 2013). Many methods including DFT, perform poorly in the case of polyatomic open-shell doublet radicals because of problems associated with the open-shell single reference wave function such as spin contamination (Hehre, 1976; Andrews et al., 1991), symmetry breaking (Davidson and Borden, 1983), near-singularities in the Hartree–Fock solution (Thouless, 1961; Čížek and Paldus, 1967), pseudo-Jahn–Teller effects (Pearson, 1976), and the presence of multi-reference character. It has been suggested that the electron of motion–coupled cluster singlet and doublet (EOM-IP-CCSD) wave function method can more accurately predict the properties of doublet radical molecules due to its incorporation of a balanced description of the dynamic and non-dynamic correlation (Saeh and Stanton, 1999; Stanton, 2007; Bravaya et al., 2012; Epifanovsky et al., 2013). Therefore, we performed geometry and harmonic frequency (presented in Table S3) calculations for NO_3 using the EOM-IP-CCSD method with the Dunning augmented correlation-consistent polarized valence double ζ (aug-cc-pVDZ) basis set (Dunning, 1989), which was the limit of our computational resources. These harmonic frequencies were used to calculate the $^{15}\beta$ of NO_3 assuming no harmonic frequencies scale factor is needed for this highly electron-correlated and generally accurate method.

3.3. Calculated $^{15}\beta$

The $^{15}\beta$ of all gaseous NO_y compounds were calculated over the temperature range of 150–450 K for each computational method used in this study. Table 1 presents the regression parameters for the temperature dependence of $^{15}\beta$ for the nineteen gaseous NO_y molecules in order of increasing magnitude for ^{15}N substitution at 150 K. In general, the magnitude of $^{15}\beta$ increases roughly with the number of atoms bonded to a particular N atom within a molecule. The smallest $^{15}\beta$ values are found for NO, NOBr, and NOCl since in the case of these molecules, N is only bonded to one other atom. The largest $^{15}\beta$ values are found in NO_3^-, HNO_3, PAN, and HNO_4, and in all of these molecules, N is bonded to three other atoms. The ordering of $^{15}\beta$ values for N containing molecules that have the same number of atoms bonded to N, depends on the bond strength and bond order between N and the atom or atoms to which it is bonded.

In Fig. 3, $^{15}\beta$ of NO, NO_2, N_2O^{α}, and HNO_3 are compared with those estimated by other empirical force field methods (Bigeleisen and Friedman, 1950; Monse et al., 1969) and available experimental harmonic frequency data (Chedin et al., 1976; Richet et al., 1977). For N_2O the α signifies ^{15}N substitution in the terminal N atom (^{15}N–^{14}N–O). The experimental harmonic frequencies for the ^{14}N and ^{15}N isotopologues of NO, NO_2, and N_2O^{α} and the corresponding calculated $^{15}\beta$ values can be found in the Supplementary material (Tables S4 and S5). Overall, our calculated $^{15}\beta$ values using computational quantum chemistry methods are in excellent agreement with $^{15}\beta$ values calculated using experimental harmonic frequencies, and harmonic frequencies calculated from molecular force fields and geometries. Therefore, we expect that our chosen levels of theory for the calculation of $^{15}\beta$ values are fairly accurate and will enable the calculation for various other NO_y molecules in which harmonic frequencies are challenging to measure experimentally.

3.4. Calculated $\alpha_{A/B}$

The calculated $\alpha_{A/B}$ regression coefficients as a function of temperature (Table 2) for the following exchange processes in the gas phase (A ↔ B): NOCl ↔ NO, HNO_2 ↔ NO, N_2O_5 ↔ NO_2, N_2O_4 ↔ NO_2, $ClNO_2$ ↔ NO_2, NO_2 ↔ NO, PAN ↔ NO_2, and HNO_3 ↔ NO in increasing order of magnitude over the temperature range of 150–450 K for the B3LYP and EDF2 methods. Since $^{15}\beta$ values for individual N-bearing molecules involved in the equilibrium isotope exchange process dictates the value of $\alpha_{A/B}$, the smallest values occur for equilibrium isotope exchange in which the number of atoms N is bonded to does not change. Thus, of the exchange processes assessed, NOCl ↔ NO had the lowest $\alpha_{A/B}$ value because in both cases, N is bonded to the same number of atoms in both molecules involved in the exchange (1 in NOCl ↔ NO). Conversely, the isotope exchange between HNO_3 ↔ NO had the highest $\alpha_{A/B}$ of those assessed, because the exchange involves N bonded to either one other atom (NO) or 3 other atoms (HNO_3). This general trend may allow for a *priori* way to predict the direction and magnitude of $\alpha_{A/B}$ based on molecular structure. This could be useful in predicting the direction of ^{15}N enrichment in other equilibrium isotope exchange processes involving N, and could be useful in evaluating kinetic isotope effects (KIE) involving N isotopologues assuming that the transition state and reactants exists in equilibrium (Van Hook, 2011). For example, a N-bearing molecule that reacts with another molecule causing the N atom to form an additional bond in the transition state would favor the formation of ^{15}N isotopologue in the transition state, which could lead to inverse kinetic isotope effects.

To assess the accuracy of our calculated values, $\alpha_{A/B}$ for $NOCl_{(l)}$ ↔ NO, NO_2 ↔ NO, $HNO_{3(aq)}$ ↔ NO, and $N_2O_{4(aq)}$ ↔ NO_2 were compared with those estimated by other theoretical studies (Begun and Fletcher, 1960; Monse et al., 1969), measured values (Leifer, 1940; Begun, 1956; Begun and Melton, 1956; Yeatts, 1958; Brown and Begun, 1959; Kauder et al., 1959), and/or available experimental harmonic frequency data (Richet et al., 1977) (Fig. 4). Due to the difficulty in measuring the $\alpha_{A/B}$ for exchange reactions involving NO_y molecules, few measurements have been made, and the majority of those that have been involve a molecule in a condensed phase (aqueous or liquid phase). Here, we neglect the condensed phase or solvent effect for a couple of reasons (1) to compare our computational determined values with those in previous theoretical studies that have also neglected solvent effects (2) to evaluate the solvent effect on $^{15}\beta$ and on $\alpha_{A/B}$ in Section 3.5. Both DFT methods resulted in extremely similar $\alpha_{A/B}$ values for all exchanges considered (Fig. 4). In general, the DFT calculated $\alpha_{A/B}$ values were in good agreement with experimental measurements (Fig. 4) and better

Table 1
Calculated regression coefficients for $^{15}\beta$ for gaseous NO_y molecules as a function of temperature (150–450 K) sorted in order of increasing magnitude at 150 K.

	$1000(\beta-1)=\frac{A}{T^4}\times10^{10}+\frac{B}{T^3}\times10^{8}+\frac{C}{T^2}\times10^{6}+\frac{D}{T}\times10^{4}$											
	B3LYP/cc-pVTZ				EDF2/cc-pVTZ				Average			
	A	B	C	D	A	B	C	D	A	B	C	D
NO	5.525	−9.890	6.753	0.701	5.530	−9.898	6.759	0.707	5.528	−9.894	6.756	0.704
NOBr	5.605	−10.072	7.288	0.790	5.758	−10.344	7.490	0.811	5.682	−10.208	7.389	0.800
NOCl	5.617	−10.109	7.346	0.815	5.617	−10.113	7.357	0.814	5.617	−10.111	7.351	0.814
N_2O^{α}	6.211	−11.627	8.834	0.723	6.222	−11.647	8.844	0.718	6.217	−11.637	8.839	0.721
$N_2O_3^{\alpha}$	5.845	−11.043	8.862	0.611	5.863	−11.079	8.893	0.614	5.854	−11.061	8.878	0.613
HNO_2	6.694	−12.953	10.370	0.432	6.767	−13.087	10.467	0.434	6.730	−13.020	10.419	0.433
NO_2^-	8.394	−15.994	12.228	0.189	8.484	−16.136	12.315	0.201	8.439	−16.065	12.271	0.195
NO_2	9.098	−16.947	12.886	0.560	9.127	−17.005	12.933	0.560	9.113	−16.976	12.909	0.560
$N_2O_3^{avg}$	7.796	−14.668	11.981	0.586	7.836	−14.732	12.035	0.602	7.816	−14.700	12.008	0.594
N_2O^{avg}	6.901	−13.012	10.796	1.001	6.923	−13.038	10.783	1.014	6.912	−13.025	10.789	1.008
NO_3^{*}									8.024	−15.955	13.722	0.077
$N_2O_3^{\beta}$	9.746	−18.293	15.101	0.560	9.809	−18.385	25.177	0.589	9.778	−18.339	15.139	0.574
N_2O^{β}	7.590	−14.397	12.758	1.280	7.625	−14.430	12.721	1.309	7.607	−14.414	12.740	1.295
$BrNO_2$	9.374	−17.846	15.287	0.616	9.427	−17.919	15.348	0.645	9.400	−17.882	15.318	0.631
$ClNO_2$	9.382	−18.029	15.568	0.553	9.463	−18.155	15.675	0.582	9.423	−18.092	15.621	0.567
N_2O_5	9.742	−18.484	15.585	0.671	9.823	−18.609	15.689	0.702	9.782	−18.547	15.637	0.687
N_2O_4	10.066	−18.947	16.032	0.711	10.049	−18.958	16.065	0.687	10.057	−18.952	16.049	0.699
$ClONO_2$	9.974	−19.144	16.582	0.592	10.041	−19.243	16.669	0.620	10.008	−19.194	16.626	0.606
$BrONO_2$	10.209	−19.552	16.922	0.605	10.306	−19.706	17.054	0.631	10.257	−19.629	16.988	0.618
HNO_4	10.407	−19.894	17.111	0.605	10.497	−20.033	17.227	0.636	10.452	−19.963	17.169	0.621
PAN	10.291	−19.611	16.934	0.672	10.384	−19.757	17.063	0.703	10.338	−19.584	16.998	0.667
HNO_3	11.120	−21.270	18.132	0.519	11.219	−21.427	18.253	0.540	11.169	−21.349	18.193	0.529
NO_3^-	12.466	−23.715	19.765	0.303	12.601	−23.918	19.905	0.326	12.533	−23.817	19.835	0.315

The typical misfit of the regression line is 0.10‰.
$^{\alpha}$ Signifies terminal substitution of ^{15}N (^{15}N–^{14}N-O and O-^{15}N-^{14}N-O_2).
$^{\beta}$ Signifies central substitution of ^{15}N (^{14}N–^{15}N-O and O-^{14}N-^{15}N-O_2).
* EOM-IP-CCSD/aug-cc-pVTZ level of theory was used to calculated $^{15}\beta$ for NO_3.

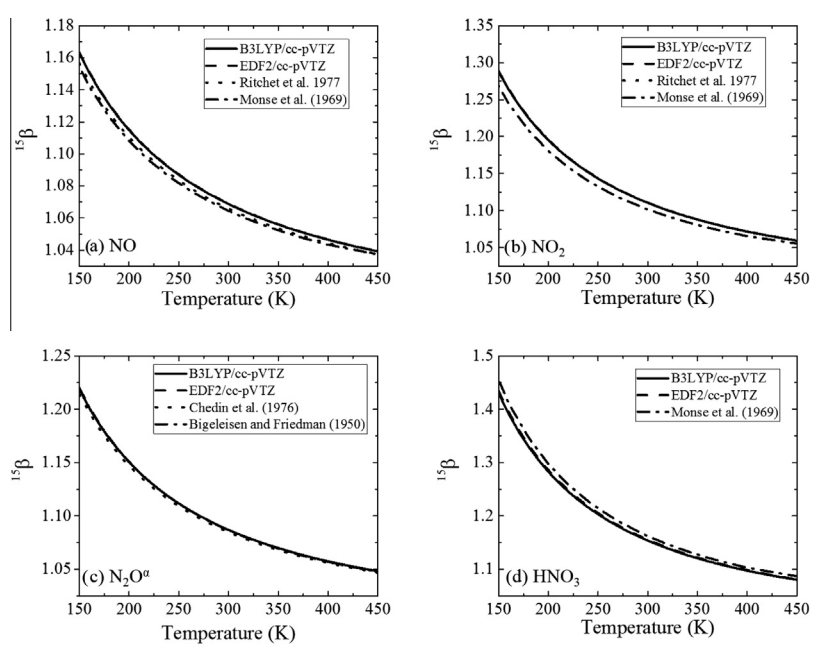

Fig. 3. Comparison of calculated gaseous $^{15}\beta$ values using B3LYP/cc-pVTZ (solid line) and EDF2/cc-pVTZ (dash line) methods with those computed in a previous study (dash dot line) and/or those computed from experimental harmonic frequencies (dot line) for (a) NO, (b) NO_2, (c) N_2O^{α}, and (d) HNO_3.

Table 2
Calculated regression coefficients for $\alpha_{A/B}$ involving gaseous NO_y molecules as a function of temperature (150–450 K) sorted in increasing magnitude at 150 K.

	$1000(\alpha_{A-B}-1)=\frac{A}{T^4}\times10^{10}+\frac{B}{T^3}\times10^{8}+\frac{C}{T^2}\times10^{6}+\frac{D}{T}\times10^{4}$											
	B3LYP/cc-pVTZ				EDF2/cc-pVTZ				Average			
	A	B	C	D	A	B	C	D	A	B	C	D
$\alpha_{NOCl-NO}$	0.121	−0.345	0.568	0.116	0.118	−0.345	0.575	0.110	0.120	−0.345	0.572	0.113
α_{HNO_2-NO}	1.447	−3.655	3.643	−0.263	1.518	−3.788	3.731	−0.266	1.483	−3.721	3.687	−0.265
$\alpha_{N_2O_5-NO_2}$	0.979	−2.487	2.697	0.119	1.030	−2.563	2.738	0.152	1.004	−2.525	2.718	0.135
$\alpha_{N_2O_4(aq)-NO_2}$	0.967	−2.515	2.843	0.053	0.879	−2.336	2.701	0.073	0.923	−2.426	2.772	0.063
$\alpha_{N_2O_4-NO_2}$	1.297	−3.019	3.110	0.163	1.262	−2.986	3.110	0.138	1.279	−3.003	3.110	0.150
$\alpha_{ClONO_2-NO_2}$	1.353	−3.484	3.734	0.040	1.390	−3.534	3.762	0.069	1.372	−3.509	3.748	0.054
α_{PAN-NO_2}	1.664	−3.979	4.032	0.125	1.730	−4.084	4.098	0.158	1.697	−4.031	4.065	0.142
α_{NO_2-NO}	3.834	−7.653	5.983	−0.115	3.861	−7.708	6.024	−0.121	3.847	−7.680	6.003	−0.118
$\alpha_{HNO_3(aq)-NO}$	6.119	−12.759	11.162	−0.141	6.079	−12.742	11.158	−0.218	6.099	−12.750	11.160	−0.179
α_{HNO_3-NO}	6.119	−12.759	11.162	−0.141	6.213	−12.914	11.267	−0.124	6.166	−12.836	11.215	−0.133

The typical misfit of the regression line is 0.20‰.

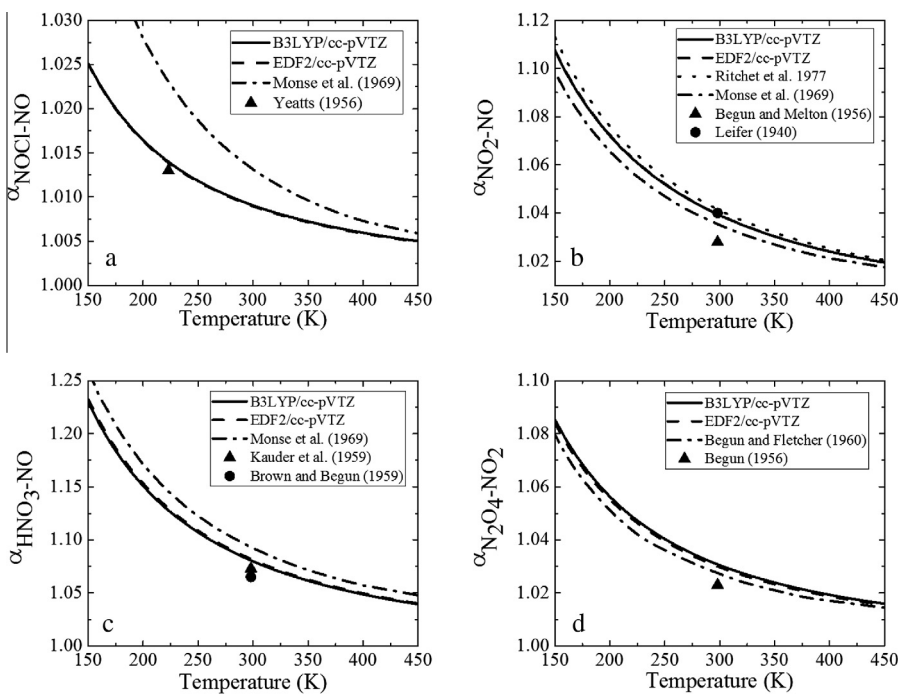

Fig. 4. Comparison of calculated equilibrium isotope fractionation factors using B3LYP/cc-pVTZ (solid line) and EDF2/cc-pVTZ (dash line) methods with neglect of solvent effects with those computed from experimental harmonic frequencies (dot line), those computed in previous studies (dash dot line) and/or those experimental measured (single points) for (a) $\alpha_{NOCl-NO}$, (b) α_{NO_2-NO}, (c) α_{HNO_3-NO}, and (d) $\alpha_{N_2O_4-NO_2}$.

estimated the $\alpha_{A/B}$ values than previous theoretical studies (Monse et al., 1969). A detailed discussion of the various exchange processes used to compare our calculated $\alpha_{A/B}$ with those previously calculated is presented below.

$\alpha_{NOCl(l)-NO}$: The N isotope exchange reaction between $NOCl_{(l)} \leftrightarrow NO$ has been previously measured to have an $\alpha_{NOCl(l)-NO}$ value of 1.013 ± 0.003 at 223 K (Yeatts, 1958). This value is an excellent agreement with the $\alpha_{NOCl-NO}$ calculated from the DFT methods which had an average value of 1.014 at 223 K (Fig. 4a) even with the neglect of the condensed phase, suggesting that the condensed phase has little influence on $^{15}\beta$ for NOCl. Our calculated $\alpha_{NOCl-NO}$ seems to significantly improve upon previous theoretical studies of this exchange reaction that calculated a value of 1.024 (Monse et al., 1969).

α_{NO_2-NO}: There has been some uncertainty in the measurement of the $\alpha_{A/B}$ for the N isotope exchange between $NO_2 \leftrightarrow NO$, one of the few N isotope exchanges that has been measured in which both molecules are in the gas phase. The earliest study of this isotope equilibrium exchange measured an α_{NO_2-NO} of 1.040 at 298 K (Leifer, 1940). This value agrees well with the α_{NO_2-NO} calculated using DFT methods that had an average value of 1.0395 at 298 K, which is also near the α_{NO_2-NO} calculated using

experimental harmonic frequencies for the ^{14}N and ^{15}N isotopologues of NO and NO_2 of 1.0415 (Richet et al., 1977), and a previous study that corrected for accurate ZPEs and calculated 1.040 (Begun and Fletcher, 1960) (Fig. 4b). However, a subsequent study found this exchange to have a $\alpha_{NO_2\text{-}NO}$ value of 1.028 ± 0.002 at 298 K (Begun and Melton, 1956). A previous theoretical study based on empirical force field calculations estimated an $\alpha_{NO_2\text{-}NO}$ value of 1.0353 (Monse et al., 1969), somewhere in between the two experimental measurements. Experimental measurements of the N isotope exchange between $NO_2 \leftrightarrow NO$ are difficult due to a number of reasons. First, the pressure of NO and NO_2 must remain low (less than 0.5 Torr) to prevent the formation of N_2O_3 and N_2O_4 (Hurtmans et al., 1993), which would complicate the $NO_2 \leftrightarrow NO$ exchange measurement. Additionally, previous studies have measured this exchange by flowing gaseous NO_2 and NO into a mass spectrometer (Leifer, 1940; Begun and Melton, 1956), but the separate mass analysis for the NO_2 and NO peaks is complicated due to the formation of NO^+ and NO_2^+ ions that originate from NO_2. Due to the small number of measurements and disagreement in these values, it is difficult to justifiable determine the accuracy of our calculated $\alpha_{NO_2\text{-}NO}$ value; however, our value does agree quite well with the value determined from the experimental harmonic frequencies, which is the best that we could hope for considering that the accuracy of our calculated $\alpha_{NO_2\text{-}NO}$ is based essentially on calculating accurate harmonic frequencies. The determination of $\alpha_{A/B}$ for this exchange reaction at various temperatures that circumvents the problems associated with previous experiments will be the subject for a future study.

$\alpha_{HNO_3(aq)\text{-}NO}$: The N isotope exchange between $HNO_{3(aq)} \leftrightarrow NO$ has been experimentally measured to have an $\alpha_{HNO_3(aq)/NO}$ of 1.073 ± 0.006 (Kauder et al., 1959) and 1.065 ± 0.001 (Brown and Begun, 1959) at 298 K. The DFT methods calculated an average $\alpha_{HNO_3/NO}$ of 1.081(Fig. 4c). While our calculated $\alpha_{HNO_3/NO}$ slightly overestimates the experimental value, it is closer than the previously calculated $\alpha_{HNO_3/NO}$ value of 1.093 based on empirical force field methods (Monse et al., 1969). It is important to point out that the $HNO_{3(aq)} \leftrightarrow NO$ exchange occurs with HNO_3 in the aqueous phase, and this could be the reason for the DFT methods overestimation of $\alpha_{HNO_3/NO}$, which assumes both HNO_3 and NO are in the gaseous phase. This isotope exchange process was re-evaluated in 3.5 using the $^{15}\beta$ calculated for $HNO_{3(aq)}$.

$\alpha_{N_2O_4(aq)\text{-}NO_2}$: The N isotope exchange reaction between $N_2O_{4(aq)} \leftrightarrow NO_2$ has been experimentally measured to have an $\alpha_{N_2O_4\text{-}NO_2}$ of 1.023 at 298 K (Begun, 1956). This value is slightly lower than the average value calculated using DFT methods of 1.030. At 298 K, Begun and Fletcher (1960) calculated $\alpha_{N_2O_4\text{-}NO_2}$ to be 1.027 which is closer to the experimental value than the DFT methods (Fig. 4d). However, Begun and Fletcher calculated $^{15}\beta$ for N_2O_4 using observed fundamental vibrational frequencies, which theoretically should not be used in the Bigeleisen–Mayer equation in the rigid rotor and harmonic oscillator approximations (Liu et al., 2010). Additionally, the calculation of $^{15}\beta$ values from observed frequencies suffers the disadvantage that spectroscopic vibrational frequencies for isotopologues are not always that accurate, and the Teller–Redlich product rule is not necessarily obeyed so that the important interplay of various factors such as mass-moment-of-inertia factor and excitation factor that contribute to $^{15}\beta$ does not necessarily occur to sufficient accuracy (Spindel and Stern, 1969). Therefore, Begun and Fletcher's more accurate calculated $\alpha_{N_2O_4\text{-}NO_2}$ maybe fortuitous. Similarly to the $HNO_{3(aq)} \leftrightarrow NO$ exchange, the experimental measurement of $N_2O_{4(aq)} \leftrightarrow NO_2$ occurred with N_2O_4 in the aqueous phase, and our calculated $^{15}\beta$ N_2O_4 used in our $\alpha_{N_2O_4\text{-}NO_2}$ calculation was for N_2O_4 in the gas phase. The difference in the phase of N_2O_4 might be the reason for our calculated $\alpha_{A/B}$ discrepancy with the experimentally measured value. In Section 3.5, the N_2O_4 aqueous phase $^{15}\beta$ value was calculated and the exchange between $N_2O_4 \leftrightarrow NO_2$ was reevaluated.

Overall, we believe that our calculated $^{15}\beta$ values for gaseous NO_y molecules are fairly accurate in the rigid rotor and harmonic oscillator approximations and will allow for the determination of $\alpha_{A/B}$ for various isotope exchanges involving these gaseous molecules. These $\alpha_{A/B}$ values maybe useful to understand the trends observed in the N stable isotope ratio of NO_y species in the atmosphere.

3.5. Calculated solvent effects

The vibrational frequencies for aqueous phase HNO_2, HNO_3, HNO_4, N_2O_3, N_2O_4, N_2O_5, NO_2^-, and NO_3^- are presented in Supplementary material (Table S6), and Table 3 presents the regression parameters for the temperature dependence of $^{15}\beta$ for these molecules in order of increasing magnitude for ^{15}N substitution. Like the gaseous NO_y molecules, $^{15}\beta$ values increase in magnitude with increasing number of atom attachment to the N atom. To assess the significance of solvent effects on $^{15}\beta$ values, Fig. 5 shows the calculated enrichment factors ($1000(\alpha_{aq\text{-}gas} - 1)$) between five gaseous NO_y molecules and their aqueous counterparts (i.e., the IEF-PCM modeled species, $\varepsilon = 78.39$) as a function of temperature. Overall, both B3LYP/cc-pVTZ and EDF2/cc-pVTZ calculated similar enrichment factors that were slightly negative between the aqueous and gaseous phase for these molecules that asymptotically increase as temperature increases but with varying magnitude for different NO_y molecules. This indicates that the $^{15}\beta$ values for the gaseous phase is higher than for the aqueous phase, signifying that the ^{15}N isotope preferentially form in the gaseous phase. This occurs because the aqueous phase lowers the ZPEs between the ^{14}N and ^{15}N isotopologues compared to the gaseous phase (Table 4) due to the stabilization resulting from dispersion interactions between water and the NO_y molecule. Subsequently, the $^{15}\beta$ value for the aqueous phase is lower than for the gaseous phase. The magnitude in the fractionation between the aqueous and gaseous phase in general depends on the ZPE difference between the ^{14}N and ^{15}N isotopologues of the aqueous and gaseous phase; the greater the ZPE is lowered in the aqueous phase, the larger the fractionation between the aqueous and gas phase (Table 4).

Table 3
Calculated regression coefficients for $^{15}\beta$ for aqueous NO_y molecules as a function of temperature (150–450 K) in order of increasing magnitude at 150 K.

	$1000(^{15}\beta - 1) = \frac{A}{T^4} \times 10^{10} + \frac{B}{T^3} \times 10^8 + \frac{C}{T^2} \times 10^6 + \frac{D}{T} \times 10^4$											
	B3LYP/cc-pVTZ				EDF2/cc-pVTZ				Average			
	A	B	C	D	A	B	C	D	A	B	C	D
$N_2O_3^{\alpha}$	5.832	−10.982	8.780	0.638	5.854	−11.031	8.831	0.635	5.843	−11.006	8.805	0.636
HNO_2	6.640	−12.915	10.386	0.373	6.740	−13.097	10.514	0.375	6.690	−13.006	10.450	0.374
NO_2^-	8.159	−15.617	11.997	0.164	8.257	−15.773	12.092	0.176	8.208	−15.695	12.044	0.170
$N_2O_3^{avg}$	7.701	−14.999	11.800	0.553	7.754	−14.588	11.877	0.569	7.727	−14.544	11.836	0.561
$N_2O_3^{\beta}$	9.570	−18.018	14.811	0.469	9.654	−18.146	14.924	0.502	9.612	−18.082	14.867	0.486
N_2O_5	9.373	−17.818	14.944	0.628	9.468	−17.973	15.081	0.658	9.420	−17.896	15.013	0.643
N_2O_4	9.724	−18.455	15.698	0.608	9.676	−18.357	15.606	0.627	9.700	−18.406	15.652	0.617
HNO_4	10.054	−19.345	16.708	0.528	10.152	−19.495	16.828	0.560	10.103	−19.420	16.768	0.544
HNO_3	10.950	−21.059	17.972	0.429	11.071	−21.253	18.114	0.449	11.011	−21.156	18.043	0.439
NO_3^-	11.928	22.889	19.197	0.232	12.086	−23.128	19.358	0.255	12.007	−23.009	19.278	0.243

$^{\alpha}$ Signifies terminal substitution of ^{15}N (O-^{15}N-^{14}N-O_2).
$^{\beta}$ Signifies central substitution of ^{15}N (O-^{14}N-^{15}N-O_2).
avg signifies the geometric average of $^{15}\beta$ for N_2O_3.
The typical misfit of the regression line is 0.10‰.

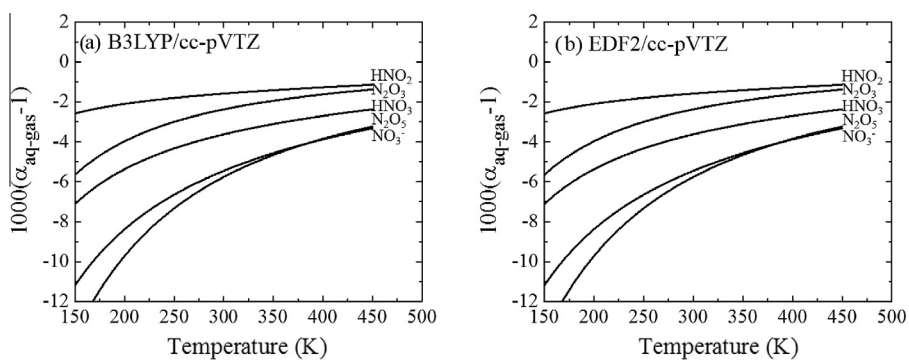

Fig. 5. Enrichment factor ($1000(\alpha_{aq\text{-}gas} - 1)$) between aqueous and gaseous phase for various NO_y molecules (HNO_2, N_2O_3, HNO_3, NO_5, NO_3^-). Aqueous phase molecules were calculated using the IEP-PCM model with a dielectric (ε) constant of 78.39.

Table 4
Comparison of the zero-point energy (ZPE = $1/2\Sigma h\nu$ for harmonic oscillators) difference in the ^{14}N and ^{15}N isotopologues for several NO_y molecules in the gaseous and the aqueous phase, and the enrichment factor ($1000\ (\alpha_{aq\text{-}gas} - 1)$) between the gaseous and aqueous phases at 270 K.

Molecule	Δ^aZPE Gas (J/mol)	Δ^aZPE Aqueous (J/mol)	Δ^aZPE Aqueous-Gas (J/mol)	$1000\ (\alpha_{aq\text{-}gas} - 1)$ at 270 K
HNO_2	324.9	322.8	−2.1	−1.6
NO_2^-	329.9	327.5	−2.4	−2.3
N_2O_3	401.7	395.1	−6.6	−2.6
HNO_3	546.0	537.2	−8.8	−4.0
HNO_4	536.9	524.9	−12.0	−5.3
N_2O_4	516.9	504.0	−12.8	−5.4
NO_3^-	556.9	543.0	−13.9	−6.1
N_2O_5	532.1	513.1	−19.0	−6.5

[a] Δ is the average difference between the ZPE in the harmonic oscillator approximation for the ^{14}N and ^{15}N isotopologues (^{14}N-^{15}N) for both B3LYP/cc-pVTZ and EDF2/cc-pVTZ levels of theory.

From the aqueous phase calculated $^{15}\beta$ for HNO_3 and N_2O_4, the N equilibrium isotope exchange between $HNO_{3(aq)} \leftrightarrow NO$ and $N_2O_{4(aq)} \leftrightarrow NO_2$ were reevaluated and compared with previous theoretical studies as well as experimental measurements (Fig. 6). A detailed assessment of the inclusion of the solvent effect on equilibrium isotope exchange processes are discussed below.

$\alpha_{HNO_3(aq)\text{-}NO}$: As previously mentioned, the N isotope exchange between $HNO_{3(aq)} \leftrightarrow NO$ has been experimentally measured to have an $\alpha_{HNO_3(aq)/NO}$ of 1.073 ± 0.006 (Kauder et al., 1959) and 1.065 ± 0.001 (Brown and Begun, 1959) at 298 K. Inclusion of the solvent effect on $^{15}\beta$ for HNO_3, the DFT methods calculated $\alpha_{HNO_3(aq)/NO}$ to be 1.076 (Fig. 6a), which is closer to the experimentally

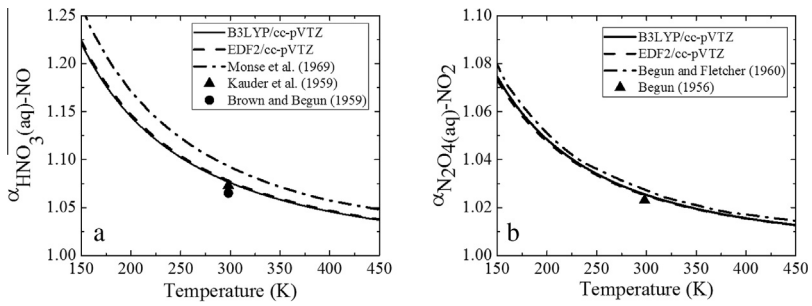

Fig. 6. Comparison of calculated equilibrium isotope fractionation factors using B3LYP/cc-pVTZ (solid line) and EDF2/cc-pVTZ (dash line) methods with inclusion of solvent effects using the IEF-PCM model with those computed in previous studies (dash dot line) and/or those experimental measured (individual points) for (a) $\alpha_{HNO_3\text{-}NO}$ and (b) $\alpha_{N_2O_4\text{-}NO_2}$.

measured values than the DFT value calculated with neglect of the solvent effect of 1.081 ± 0.001 (Fig. 6a). Our calculated $\alpha_{HNO_3(aq)/NO}$ value is a significant improvement from previous theoretical studies that have calculated a value of 1.093 (Monse et al., 1969).

$\alpha_{N_2O_4(aq)\text{-}NO_2}$: Inclusion of the solvent effect on the $^{15}\beta$ value of N_2O_4, the DFT methods calculated $\alpha_{N_2O_4(aq)\text{-}NO_2}$ to be 1.025(Fig. 6b). This value is in better agreement with the experimentally determined value of 1.023 (Begun, 1956) than either the DFT calculated value with neglect of the solvent effect of 1.034 ± 0.0005 or the value calculated using observed fundamental vibrational frequencies of 1.027 (Begun and Fletcher, 1960).

Overall, the solvent effect while not very strong, are still significant for calculating accurate fractionation factors. Inclusion of the solvent effect for the molecules analyzed in this study lowered $\alpha_{A/B}$ and resulted in values closer in agreement with experimentally determined values. Even with accounting for solvent effects, calculated $\alpha_{A/B}$ in the rigid rotor and harmonic oscillator approximations tend to be slightly overestimated compare to the experimentally measured value, and this is likely due to the neglect of anharmonicity in this approximation. Inclusion of anharmonic corrections will in general lower $\alpha_{A/B}$ values, which would help match calculated values with those determined experimentally; however, corrections for anharmonicity are computationally expensive, and even with the neglect of anharmonicity, our calculated $\alpha_{A/B}$ values are within or nearly within the experimental error for these measurements and are a significant improvement from previous theoretical $\alpha_{A/B}$ studies involving NO_y molecules.

4. CONCLUSIONS

Harmonic frequencies have been calculated for various NO_y molecules that are relevant to NO_x tropospheric and stratospheric chemistry using B3LYP/cc-pVTZ and EDF2/cc-pVTZ levels of theory. Our calculated harmonic frequencies were in excellent agreement with those determined experimentally. Using our calculated harmonic frequencies, $^{15}\beta$ were calculated for mono-substitution of the ^{15}N isotope using the Bigeleisen–Mayer equation in the rigid rotor and harmonic oscillator approximations. Our $^{15}\beta$ values agreed well with those calculated using experimentally determined harmonic frequencies and with those calculated using empirical force field methods. In general, the magnitude of $^{15}\beta$ value increases with the number of atoms bound to the N atom in a particular molecule, allowing for a *priori* way to arrange $^{15}\beta$ values for NO_y molecules. Equilibrium isotope exchange fractionation factors ($\alpha_{A/B}$) were evaluated for various exchange processes involving NO_y molecules. Our calculated $\alpha_{A/B}$ values were generally in closer agreement with the experimentally measured $\alpha_{A/B}$ than previous theoretical assessments of $\alpha_{A/B}$ involving N isotope exchange. Since most of the $\alpha_{A/B}$ values involving N isotope exchange involved a species in the aqueous phase, the solvent effect on $^{15}\beta$ and $\alpha_{A/B}$ were assessed. Inclusion of the solvent effect improved the accuracy of our calculated $\alpha_{A/B}$ values so that they were just outside of or within the experimental variability reported for various N isotope exchange processes. Slight overestimations even after corrections for the solvent effect might be the result of neglect of anharmonicity which are believed to lower $\alpha_{A/B}$ values. In general, we believe our calculated $^{15}\beta$ and $\alpha_{A/B}$ values are accurate in the rigid rotor and harmonic oscillator approximations and will allow for the estimation of the isotope fractionation involved with NO_y molecules.

These $\alpha_{A/B}$ values predict trends that may be observed in the N stable isotope ratio of NO_y species in the atmosphere. Assuming that NO_y species exists in equilibrium, this would suggest (1) since the ^{15}N isotope prefers to enrich in the more oxidized form of NO_y, the transformation of NO_x to atmospheric nitrates (HNO_3, $NO_{3\,(aq)}^-$, $NO_{3\,(g)}^-$) would increase the $^{15}N/^{14}N$ ratios from the initial $^{15}N/^{14}N$ ratio of the NO_x source, (2) the long range transport of NO_x via PAN would have higher $^{15}N/^{14}N$ ratios than the NO_x source, (3) based on $^{15}\beta$ values, atmospheric nitrates would have $^{15}N/^{14}N$ ratios in order of increasing magnitude of $NO_{3\,(aq)}^-$, HNO_3, $NO_{3\,(s)}^-$. Simultaneous measurements of the $^{15}N/^{14}N$ ratios of different NO_y molecules is needed to determine the importance of various equilibrium isotope exchanges on $^{15}N/^{14}N$ ratios, and this will be the subject for future research.

ACKNOWLEDGEMENTS

W.W.W. was a National Science Foundation Graduate Research Fellow during the course of the study. We would like

to thank the Purdue Climate Change Research Center (PCCRC) graduate fellowship program for supporting this work. The authors grateful acknowledge Dr. Alexander Van Hook and one anonymous reviewer for their helpful comments.

APPENDIX A. SUPPLEMENTARY DATA

Supplementary data associated with this article can be found, in the online version, at http://dx.doi.org/10.1016/j.gca.2015.05.029.

REFERENCES

Ammann M., Siegwolf R., Pichlmayer F., Suter M., Saurer M. and Brunold C. (1999) Estimating the uptake of traffic-derived NO_2 from ^{15}N abundance in Norway spruce needles. *Oecologia* **118**, 124–131.

Anbar A. D., Jarzecki A. A. and Spiro T. G. (2005) Theoretical investigation of iron isotope fractionation between $Fe(H_2O)_6^{3+}$ and $Fe(H_2O)_6^{2+}$: implications for iron stable isotope geochemistry. *Geochim. Cosmochim. Acta* **69**, 825–837.

Andrews J. S., Jayatilaka D., Bone R. G., Handy N. C. and Amos R. D. (1991) Spin contamination in single-determinant wavefunctions. *Chem. Phys. Lett.* **183**, 423–431.

Atkinson R. (2000) Atmospheric chemistry of VOCs and NO_x. *Atmos. Environ.* **34**, 2063–2101.

Barone V. and Cossi M. (1998) Quantum calculation of molecular energies and energy gradients in solution by a conductor solvent model. *J. Phys. Chem. A* **102**, 1995–2001.

Becke A. D. (1993) Density-functional thermochemistry. III. The role of exact exchange. *J. Chem. Phys.* **98**, 5648–5652.

Begun G. M. (1956) Nitrogen isotope effect in the distillation of N_2O_4. *J. Chem. Phys.* **25**, 1279–1280.

Begun G. M. and Fletcher W. H. (1960) Partition function ratios for molecules containing nitrogen isotopes. *J. Chem. Phys.* **33**, 1083–1085.

Begun G. M. and Melton C. E. (1956) Nitrogen isotopic fractionation between NO and NO_2 and mass discrimination in mass analysis of NO_2. *J. Chem. Phys.* **25**, 1292–1293.

Beyn F., Matthias V., Aulinger A. and Dähnke K. (2015) Do N-isotopes in atmospheric nitrate deposition reflect air pollution levels? *Atmos. Environ.* **107**, 281–288.

Bigeleisen J. and Friedman L. (1950) The infra-red spectra of $N^{15}N^{14}O^{16}$ and $N^{14}N^{15}O^{16}$. some thermodynamic properties of the isotopic N_2O molecules. *J. Chem. Phys.* **18**, 1656–1659.

Bigeleisen J. and Mayer M. G. (1947) Calculation of equilibrium constants for isotopic exchange reactions. *J. Chem. Phys.* **15**, 261–267.

Bravaya K. B., Epifanovsky E. and Krylov A. I. (2012) Four bases score a run: Ab initio calculations quantify a cooperative effect of H-bonding and π-stacking on the ionization energy of adenine in the AATT tetramer. *J. Phys. Chem. Lett.* **3**, 2726–2732.

Brown L. L. and Begun G. M. (1959) Nitrogen isotopic fractionation between nitric acid and the oxides of nitrogen. *J. Chem. Phys.* **30**, 1206–1209.

Cancès E., Mennucci B. and Tomasi J. (1997) A new integral equation formalism for the polarizable continuum model: theoretical background and applications to isotropic and anisotropic dielectrics. *J. Chem. Phys.* **107**, 3032–3041.

Chedin A., Amiot C. and Cihla Z. (1976) The potential energy function of the nitrous oxide molecule using pure vibrational data. *J. Mol. Spectrosc.* **63**, 348–369.

Chipman D. M. (2000) Reaction field treatment of charge penetration. *J. Chem. Phys.* **112**, 5558–5565.

Čížek J. and Paldus J. (1967) Stability conditions for the solutions of the Hartree–Fock equations for atomic and molecular systems. application to the Pi-electron model of cyclic polyenes. *J. Chem. Phys.* **47**, 3976–3985.

Cossi M., Rega N., Scalmani G. and Barone V. (2003) Energies, structures, and electronic properties of molecules in solution with the C-PCM solvation model. *J. Comput. Chem.* **24**, 669–681.

Crutzen P. J. (1979) The role of NO and NO_2 in the chemistry of the troposphere and stratosphere. *Ann. Rev. Earth Planet. Sci.* **7**, 443–472.

Crutzen P. J. and Arnold F. (1986) Nitric acid cloud formation in the cold Antarctic stratosphere: a major cause for the springtime "ozone hole". *Nature* **324**, 651–655.

Davidson E. R. and Borden W. T. (1983) Symmetry breaking in polyatomic molecules: real and artifactual. *J. Phys. Chem.* **87**, 4783–4790.

Driesner T., Ha T. K. and Seward T. M. (2000) Oxygen and hydrogen isotope fractionation by hydration complexes of Li^+, Na^+, K^+, Mg_2^+, F^-, Cl^-, and Br^-: a theoretical study. *Geochim. Cosmochim. Acta* **64**, 3007–3033.

Dunning T. H. (1989) Gaussian basis sets for use in correlated molecular calculations. I. The atoms boron through neon and hydrogen. *J. Chem. Phys.* **90**, 1007–1023.

Dutta A. K., Vaval N. and Pal S. (2013) Performance of the EOMIP-CCSD(2) method for determining the structure and properties of doublet radicals: a benchmark investigation. *J. Chem. Theory Comput.* **9**, 4313–4331.

Elliott E. M., Kendall C., Wankel S. D., Burns D. A., Boyer E. W., Harlin K., Bain D. J. and Butler T. J. (2007) Nitrogen isotopes as indicators of NO_x source contributions to atmospheric nitrate deposition across the midwestern and northeastern United States. *Environ. Sci. Technol.* **41**, 7661–7667.

Elliott E. M., Kendall C., Boyer E. W., Burns D. A., Lear G. G., Golden H. E., Harlin K., Bytnerowicz A., Butler T. J. and Glatz R. (2009) Dual nitrate isotopes in dry deposition: utility for partitioning NO_x source contributions to landscape nitrogen deposition. *J. Geophys. Res. Biogeosci.*, 114.

Epifanovsky E., Wormit M., Kuś T., Landau A., Zuev D., Khistyaev K., Manohar P., Kaliman I., Dreuw A. and Krylov A. I. (2013) New implementation of high-level correlated methods using a general block tensor library for high-performance electronic structure calculations. *J. Comput. Chem.* **34**, 2293–2309.

Felix J. D. and Elliott E. M. (2014) Isotopic composition of passively collected nitrogen dioxide emissions: vehicle, soil and livestock source signatures. *Atmos. Environ.* **92**, 359–366.

Felix J. D., Elliott E. M. and Shaw S. L. (2012) Nitrogen isotopic composition of coal-fired power plant NO_x: influence of emission controls and implications for global emission inventories. *Environ. Sci. Technol.* **46**, 3528–3535.

Fibiger D. L., Hastings M. G., Lew A. F. and Peltier R. E. (2014) Collection of NO and NO_2 for isotopic analysis of NO_x emissions. *Anal. Chem.* **86**, 12115–12121.

Foresman J. B. and Frisch A. B. (1996) *Exploring Chemistry with Electronic Structure Methods*. Gaussian Inc., Pittsburg, PA.

Freyer H. D. (1978) Seasonal trends of NH_4^+ and NO_3^- nitrogen isotope composition in rain collected at Jülich, Germany. *Tellus* **30**, 83–92.

Freyer H. D., Kley D., Volz-Thomas A. and Kobel K. (1993) On the interaction of isotopic exchange processes with photochemical reactions in atmospheric oxides of nitrogen. *J. Geophys. Res.* **98**, 14791–14796.

Galloway J. N., Dentener F. J., Capone D. G., Boyer E. W., Howarth R. W., Seitzinger S. P., Asner G. P., Cleveland C., Green P. and Holland E. (2004) Nitrogen cycles: past, present, and future. *Biogeochemistry* **70**, 153–226.

Geng L., Alexander B., Cole-Dai J., Steig E. J., Savarino J., Sofen E. D. and Schauer A. J. (2014) Nitrogen isotopes in ice core nitrate linked to anthropogenic atmospheric acidity change. *Proc. Natl. Acad. Sci.* **111**, 5808–5812.

Hastings M. G., Jarvis J. C. and Steig E. J. (2009) Anthropogenic impacts on nitrogen isotopes of ice-core nitrate. *Science* **324**, 1288–1288.

Heaton T. H. E. (1990) $^{15}N/^{14}N$ ratios of NO_x from vehicle engines and coal-fired power stations. *Tellus B* **42**, 304–307.

Hehre W. J. (1976) Ab initio molecular orbital theory. *Acc. Chem. Res.* **9**, 399–406.

Hurtmans D., Herman M. and Vander Auwera J. (1993) Integrated band intensities in N_2O_4 in the infrared range. *J. Quant. Spectrosc. Radiat. Transfer.* **50**, 595–602.

Irikura K. K. (2007) Experimental vibrational zero-point energies: diatomic molecules. *J. Phys. Chem. Ref. Data* **36**, 389–397.

Jensen F. (1999) *Introduction to Computational Chemistry*. Wiley, New York.

Kauder L. N., Taylor T. I. and Spindel W. (1959) Isotope enrichment factors for nitrogen-15 in the nitric oxide-nitric acid exchange system. *J. Chem. Phys.* **31**, 232–235.

Klamt A. and Schüürmann G. (1993) COSMO: a new approach to dielectric screening in solvents with explicit expressions for the screening energy and its gradient. *J. Chem. Soc. Perkin Trans.* **2**, 799–805.

Lasaga A. C. (1990) Atomic treatment of mineral-water surface reactions. *Rev. Mineral. Geochem.* **23**, 17–85.

Lasaga A. C. (1998) *Kinetic Theory in the Earth Sciences*. Princeton University Press, Princeton, NJ.

Lawrence M. G. and Crutzen P. J. (1999) Influence of NO_x emissions from ships on tropospheric photochemistry and climate. *Nature* **402**, 167–170.

Lee C., Yang W. and Parr R. G. (1988) Development of the Colle-Salvetti correlation-energy formula into a functional of the electron density. *Phys. Rev. B* **37**, 785.

Leifer E. (1940) The exchange of oxygen between NO and NO_2. *J. Chem. Phys.* **8**, 301–303.

Li D. and Wang X. (2008) Nitrogen isotopic signature of soil-released nitric oxide (NO) after fertilizer application. *Atmos. Environ.* **42**, 4747–4754.

Lin C. Y., George M. W. and Gill P. M. (2004) EDF2: a density functional for predicting molecular vibrational frequencies. *Aust. J. Chem.* **57**, 365–370.

Liu Y. and Tossell J. A. (2005) Ab initio molecular orbital calculations for boron isotope fractionations on boric acids and borates. *Geochim. Cosmochim. Acta* **69**, 3995–4006.

Liu Q., Tossell J. A. and Liu Y. (2010) On the proper use of the Bigeleisen–Mayer equation and corrections to it in the calculation of isotopic fractionation equilibrium constants. *Geochim. Cosmochim. Acta* **74**, 6965–6983.

Logan J. A. (1983) Nitrogen oxides in the troposphere: global and regional budgets. *J. Geophys. Res. Oceans* **88**, 10785–10807.

Malmberg C. G. and Maryott A. A. (1956) Dielectric constant of water from 0° to 100 °C. *J. Res. Natl. Bur. Stand.* **56**, 1–8.

Mara P., Mihalopoulos N., Gogou A., Daehnke K., Schlarbaum T., Emeis K.-C. and Krom M. (2009) Isotopic composition of nitrate in wet and dry atmospheric deposition on Crete in the eastern Mediterranean Sea. *Glob. Biogeochem. Cycles* **23**, GB4002.

Melillo J. M. and Cowling E. B. (2002) Reactive nitrogen and public policies for environmental protection. *AMBIO J. Hum. Environ.* **31**, 150–158.

Michalski G. and Bhattacharya S. K. (2009) The role of symmetry in the mass independent isotope effect in ozone. *Proc. Natl. Acad. Sci.* **106**, 5493–5496.

Monse E. U., Spindel W. and Stern M. J. (1969) Analysis of isotope-effect calculations illustrated with exchange equilibria among oxynitrogen compounds. *ACS Adv. Chem.* **89**, 148–184.

Moore H. (1977) The isotopic composition of ammonia, nitrogen dioxide and nitrate in the atmosphere. *Atmos. Environ. 1967* **11**, 1239–1243.

Morris V. R., Bhatia S. C. and Hall J. H. (1990) Ab initio self-consistent field study of the vibrational spectra for nitrate radical geometric isomers. *J. Phys. Chem.* **94**, 7414–7418.

Nielsen T., Samuelsson U., Grennfelt P. and Thomsen E. L. (1981) Peroxyacetyl nitrate in long-range transported polluted air. *Nature* **293**, 553–555.

Oi T. (2000) Calculations of reduced partition function ratios of monomeric and dimeric boric acids and borates by the ab initio molecular orbital theory. *J. Nucl. Sci. Technol.* **37**, 166–172.

Oi T. and Yanase S. (2001) Calculations of reduced partition function ratios of hydrated monoborate anion by the ab initio molecular orbital theory. *J. Nucl. Sci. Technol.* **38**, 429–432.

Otake T., Lasaga A. C. and Ohmoto H. (2008) Ab initio calculations for equilibrium fractionations in multiple sulfur isotope systems. *Chem. Geol.* **249**, 357–376.

Pearson R. G. (1976) *Symmetry Rules for Chemical Reactions*. Wiley, New York.

Pearson J., Wells D. M., Seller K. J., Bennett A., Soares A., Woodall J. and Ingrouille M. J. (2000) Traffic exposure increases natural ^{15}N and heavy metal concentrations in mosses. *New Phytol.* **147**, 317–326.

Redling K., Elliott E., Bain D. and Sherwell J. (2013) Highway contributions to reactive nitrogen deposition: tracing the fate of vehicular NO_x using stable isotopes and plant biomonitors. *Biogeochemistry* **116**, 261–274.

Richet P., Bottinga Y. and Janoy M. (1977) A review of hydrogen, carbon, nitrogen, oxygen, sulphur, and chlorine stable isotope enrichment among gaseous molecules. *Ann. Rev. Earth Planet. Sci.* **5**, 65–110.

Robinson R. A. and Stokes R. H. (1959) *Electrolyte Solutions*. Academic Press, New York.

Saeh J. C. and Stanton J. F. (1999) Application of an equation-of-motion coupled cluster method including higher-order corrections to potential energy surfaces of radicals. *J. Chem. Phys.* **111**, 8275–8285.

Schauble E., Rossman G. R. and Taylor H. P. (2004) Theoretical estimates of equilibrium chromium-isotope fractionations. *Chem. Geol.* **205**, 99–114.

Seinfeld J. H. and Pandis S. N. (2006) *Atmospheric Chemistry and Physics: From air Pollution to Climate Change*. John Wiley & Sons, New York.

Seo J. H., Lee S. K. and Lee I. (2007) Quantum chemical calculations of equilibrium copper (I) isotope fractionations in ore-forming fluids. *Chem. Geol.* **243**, 225–237.

Shao Y., Gan Z., Epifanovsky E., Gilbert A. T. B., Wormit M., Kussmann J., Lange A. W., Behn A., Deng J., Feng X., Ghosh D., Goldey M., Horn P. R., Jacobson L. D., Kaliman I., Khaliullin R. Z., Kuś T., Landau A., Liu J., Proynov E. I., Rhee Y. M., Richard R. M., Rohrdanz M. A., Steele R. P., Sundstrom E. J., Woodcock H. L., Zimmerman P. M., Zuev D., Albrecht B., Alguire E., Austin B., Beran G. J. O., Bernard Y. A., Berquist E., Brandhorst K., Bravaya K. B., Brown S. T., Casanova D., Chang C.-M., Chen Y., Chien S. H., Closser K. D., Crittenden D. L., Diedenhofen M., DiStasio R. A., Do H., Dutoi A. D., Edgar R. G., Fatehi S., Fusti-Molnar L., Ghysels A., Golubeva-Zadorozhnaya A., Gomes J., Hanson-Heine M.

W. D., Harbach P. H. P., Hauser A. W., Hohenstein E. G., Holden Z. C., Jagau T.-C., Ji H., Kaduk B., Khistyaev K., Kim J., Kim J., King R. A., Klunzinger P., Kosenkov D., Kowalczyk T., Krauter C. M., Lao K. U., Laurent A. D., Lawler K. V., Levchenko S. V., Lin C. Y., Liu F., Livshits E., Lochan R. C., Luenser A., Manohar P., Manzer S. F., Mao S.-P., Mardirossian N., Marenich A. V., Maurer S. A., Mayhall N. J., Neuscamman E., Oana C. M., Olivares-Amaya R., O'Neill D. P., Parkhill J. A., Perrine T. M., Peverati R., Prociuk A., Rehn D. R., Rosta E., Russ N. J., Sharada S. M., Sharma S., Small D. W., Sodt A., Stein T., Stück D., Su Y.-C., Thom A. J. W., Tsuchimochi T., Vanovschi V., Vogt L., Vydrov O., Wang T., Watson M. A., Wenzel J., White A., Williams C. F., Yang J., Yeganeh S., Yost S. R., You Z.-Q., Zhang I. Y., Zhang X., Zhao Y., Brooks B. R., Chan G. K. L., Chipman D. M., Cramer C. J., Goddard W. A., Gordon M. S., Hehre W. J., Klamt A., Schaefer H. F., Schmidt M. W., Sherrill C. D., Truhlar D. G., Warshel A., Xu X., Aspuru-Guzik A., Baer R., Bell A. T., Besley N. A., Chai J.-D., Dreuw A., Dunietz B. D., Furlani T. R., Gwaltney S. R., Hsu C.-P., Jung Y., Kong J., Lambrecht D. S., Liang W., Ochsenfeld C., Rassolov V. A., Slipchenko L. V., Subotnik J. E., Van Voorhis T., Herbert J. M., Krylov A. I., Gill P. M. W. and Head-Gordon M. () Advances in molecular quantum chemistry contained in the Q-Chem 4 program package. *Mol. Phys.* **113**, 184–215.

Solomon S. (1999) Stratospheric ozone depletion: a review of concepts and history. *Rev. Geophys.* **37**, 275–316.

Solomon S., Qin D., Manning M., Chen Z., Marquis M., Averyt K. B., Tignor M. and Miller H. L. (2007) IPCC, 2007: Climate change 2007: The physical science basis. Contrib. Work. Group Fourth Assess. Rep. Intergov. Panel Clim. Change.

Spindel W. and Stern M. J. (1969) Comment on the fractionation of nitrogen isotopes between NO_2^- and NO_3^- and between NO and NO_2. *J. Chem. Phys.* **50**, 569–571.

Stanton J. F. (2007) On the vibronic level structure in the NO_3 radical. I. The ground electronic state. *J. Chem. Phys.* **126**, 134309.

Thouless D. J. (1961) *The Quantum Mechanics of Many-body Systems*. Academic Press, New York.

Tomasi J. and Persico M. (1994) Molecular interactions in solution: an overview of methods based on continuous distributions of the solvent. *Chem. Rev.* **94**, 2027–2094.

Tossell J. A. (2005) Calculating the partitioning of the isotopes of Mo between oxidic and sulfidic species in aqueous solution. *Geochim. Cosmochim. Acta* **69**, 2981–2993.

Truong T. N. and Stefanovich E. V. (1995) A new method for incorporating solvent effect into the classical, ab initio molecular orbital and density functional theory frameworks for arbitrary shape cavity. *Chem. Phys. Lett.* **240**, 253–260.

Urey H. C. (1947) The thermodynamic properties of isotopic substances. *J. Chem. Soc.* **7**, 562–581.

Van Hook W. A. (2011) Isotope effects in chemistry. *Nukleonika* **56**, 217–240.

Voigt C., Schreiner J., Kohlmann A., Zink P., Mauersberger K., Larsen N., Deshler T., Kröger C., Rosen J. and Adriani A., et al. (2000) Nitric acid trihydrate (NAT) in polar stratospheric clouds. *Science* **290**, 1756–1758.

Walters W. W., Goodwin S. R. and Michalski G. (2015) Nitrogen stable isotope composition ($\delta^{15}N$) of vehicle-emitted NO_x. *Environ. Sci. Technol.* **49**, 2278–2285.

Wayne R. P., Barnes I., Biggs P., Burrows J. P., Canosa-Mas C. E., Hjorth J., Le Bras G., Moortgat G. K., Perner D., Poulet G., Restelli G. and Sidebottom H. (1991) The nitrate radical: physics, chemistry, and the atmosphere. *Atmos. Environ. Part Gen. Top.* **25**, 1–203.

Yamaji K., Makita Y., Watanabe H., Sonoda A., Kanoh H., Hirotsu T. and Ooi K. (2001) Theoretical estimation of lithium isotopic reduced partition function ratio for lithium ions in aqueous solution. *J. Phys. Chem. A* **105**, 602–613.

Yeatts L. B. (1958) Fractionation of nitrogen and oxygen isotopes between gaseous NO and liquid NOCl. *J. Chem. Phys.* **28**, 1255–1255.

Associate editor: Jack J. Middelburg